Published in final edited form as:
J Biomech. 2013 April 5; 46(6): 1104–1112. doi:10.1016/j.jbiomech.2013.01.014.

The effect of patient-specific annular motion on dynamic simulation of mitral valve function

Yonghoon Rim[a], **David D. McPherson**[a], **Krishnan B. Chandran**[b], and **Hyunggun Kim**[a,b,*]

[a]Division of Cardiovascular Medicine, Department of Internal Medicine, The University of Texas Health Science Center at Houston, Houston, TX 77030, USA

[b]Department of Biomedical Engineering, The University of Iowa, Iowa City, IA 52242, USA

Abstract

Most surgical procedures for patients with mitral regurgitation (MR) focus on optimization of annular dimension and shape utilizing ring annuloplasty to restore normal annular geometry, increase leaflet coaptation, and reduce regurgitation. Computational studies may provide insight on the effect of annular motion on mitral valve (MV) function through the incorporation of patient-specific MV apparatus geometry from clinical imaging modalities such as echocardiography. In the present study, we have developed a novel algorithm for modeling patient-specific annular motion across the cardiac cycle to further improve our virtual MV modeling and simulation strategy. The MV apparatus including the leaflets, annulus, and location of papillary muscle tips was identified using patient 3D echocardiography data at end diastole and peak systole and converted to virtual MV model. Dynamic annular motion was modeled by incorporating the ECG-gated time-varying scaled annular displacement across the cardiac cycle. We performed dynamic finite element (FE) simulation of two sets of patient data with respect to the presence of MR. Annular morphology, stress distribution across the leaflets and annulus, and contact stress distribution were determined to assess the effect of annular motion on MV function and leaflet coaptation. The effect of dynamic annular motion clearly demonstrated reduced regions with large stress values and provided an improved accuracy in determining the location of improper leaflet coaptation. This strategy has the potential to better quantitate the extent of pathologic MV and better evaluate functional restoration following MV repair.

Keywords

Mitral valve; Finite element; Annular motion; Mitral regurgitation; Three-dimensional echocardiography

1. Introduction

Functional characteristics of the mitral valve (MV) are influenced by the interaction between the MV apparatus components which consist of two asymmetric leaflets, a saddle-shaped annulus, chordae tendineae, and papillary muscles (PMs) (Stevanella et al., 2009). Proper shape, size, and dynamic motion of the annulus are closely associated with normal MV function (Rausch et al., 2011a). Most surgical procedures for patients with mitral

*Corresponding author at: Division of Cardiovascular Medicine, Department of Internal Medicine, The University of Texas Health Science Center at Houston, 6431 Fannin St, MSB 1.246, Houston, TX 77030, USA. Tel.: +1 713 486 2342; fax: +1 713 500 6556. Hyunggun.Kim@uth.tmc.edu (H. Kim).

Conflict of interest statement
None of the authors has any conflict of interest.

regurgitation (MR) focus on optimization of annular dimension and shape utilizing ring annuloplasty to restore normal annular geometry, increase leaflet coaptation, and reduce regurgitation (Gorman et al., 2004; Rausch et al., 2011b).

A number of computational studies have investigated the effects of shape, size, and motion of the mitral annulus on MV function (Gorman et al., 2004; Lansac et al., 2002; Maisano et al., 2005; Rausch et al., 2011a; Votta et al., 2007). Finite element (FE) analysis has been primarily utilized to demonstrate quantitative structural alterations of the annulus. The saddle-shaped curvature of the mitral annulus provides biomechanical advantages to the MV leaflets (Salgo et al., 2002). A recent study using FE evaluation of MV models with and without moving annulus demonstrated the effect of annular motion on structural characteristics of the MV leaflets (Stevanella et al., 2009). Although these computational studies provide useful information to help us to understand important roles of the annulus in MV dynamics, it is hard to translate these data to the clinical setting without the incorporation of realistic annular motion in complex patient MV dynamics. In order to accurately evaluate the effect of annular motion on MV function, it is crucial to use patient-specific MV apparatus geometry from clinical imaging modalities.

Three-dimensional (3D) transesophageal echocardiography (TEE) is an excellent technique to accurately obtain detailed morphologic information of the MV leaflets and annulus compared to standard 2D echocardiography (currently the most popular imaging modality of clinical MV evaluation) (Hung et al., 2007; Maffessanti et al., 2011; Sonne et al., 2009; Sugeng et al., 2008; Swaans et al., 2009). It is well known that 3D TEE with high-resolution acquisition allows evaluation of mitral annular shape dynamics during the cardiac cycle (Carlhall et al., 2004). It would be expected that computational MV simulations incorporated with accurate kinematic description of annular motion from 3D TEE data can better provide biomechanical and functional MV information that may result in improved clinical diagnoses.

In this study, we have developed a novel algorithm for modeling patient-specific annular motion across the cardiac cycle to further improve our virtual MV modeling and simulation strategy. Here we have performed dynamic FE simulation of MV function using patient-specific geometry of MV leaflets, annulus, and annular motion. This study was designed to evaluate the effect of dynamic motion of the annulus on MV function over a range of clinical pathologies.

2. Materials and methods

2.1. MV modeling associated with dynamic annular motion using patient 3D TEE data

The Committee for the Protection of Human Subjects at The University of Texas Health Science Center at Houston approved this translational study which utilizes patient 3D TEE data from a clinical ultrasound unit (iE33, Philips Medical Systems, Bothell, WA). Informed consent forms were collected from the patients. Patient confidentiality was honored and patient information completely de-identified.

For the present study, 3D TEE was performed in two patients with and without MR. The study protocol to convert MV geometric data from patient 3D TEE data to a computational model followed by dynamic FE simulation with or without annular motion is shown in Fig. 1. This modeling protocol was composed of multiple sub-algorithms including 3D TEE image data acquisition, MV leaflets and apparatus segmentation, image registration, 3D reconstruction, mesh creation, chordae tendineae creation, incorporation of 3D dynamic motion of the annulus and PMs, and dynamic FE simulation of the MV function. The ECG-gated patient 3D TEE data containing the full volumetric geometry of the anterior and

posterior leaflets and annulus was transferred into a PC. MV apparatus including the leaflets and annulus was identified using patient 3D TEE data at end diastole (open). In addition to segmentation and tracing of the MV leaflets and annulus at end diastole, the annular geometry at peak systole (closed) was segmented and traced manually using a custom-designed semi-automated image processing algorithm developed with MATLAB (The Mathworks Inc., Natick, MA). The traced 3D geometric data was transformed into the Cartesian coordinate. Using the nonuniform rational B-spline (NURBS) surface modeling technique, the 3D MV leaflets and annulus were created and meshed. The PM tips were modeled continuously deforming while keeping a constant distance of 38 mm from the top of the annulus with a distance of 18 mm between the two PM tips during dynamic annular motion (Sonne et al., 2009). The chordae tendineae were modeled by adding line elements between the PM tips and the edge nodes of the MV leaflets in ABAQUS (SIMULIA, Providence, RI) software. Following incorporation of 3D dynamic motion of the annulus and PM tips, the 3D virtual MV modeling was completed.

2.2. Alignment of the annular configurations for modeling of dynamic annular motion

The annular geometries at peak systole and end diastole were imaged from the 3D TEE probe outside of the heart. It is necessary to introduce a transformation matrix to align the two annular geometric data under a single configuration to compensate the motion of the left ventricle. A schematic diagram is shown in Fig. 2A to describe the coordinate system transformation between the two annular configurations. The annular geometry at the peak systole configuration was transformed onto the end diastole configuration as follows.

The coordinate data (M) of the annular geometry at peak systole was transformed to M' at end diastole:

$$M' = T_{Comp} M \quad (1)$$

$$T_{Comp} = T_{Dia,G} T_{G,Sys} \quad (2)$$

where T_{Comp} is a 4 × 4 composite transformation matrix calculated by matrix multiplication of multiple transformations from peak systole to end diastole. The 4 × 4 transformation matrix can contain both rotational and translational transformations in a single matrix. Transformations ($T_{Sys,\,G}$ and $T_{Dia,\,G}$) were defined by the angular orientation of each configuration using the reference points (denoted as points p_{Al}, p_{Pm}, p_A, p_P at peak systole and p_{Al}', p_{Pm}', p_A', p_P' at end diastole) and the translations (o_{Sys} and o_{Dia}) from the global origin (o_G) (Ganapathy, 1984; Paul, 1981). The transformation matrices can be expressed as follows:

$$T_{Sys,G} = \begin{bmatrix} & A_{Sys} & & o_{Sys} \\ 0 & 0 & 0 & 1 \end{bmatrix} \quad (3)$$

where

$$o_{Sys} = (p_{Al} - p_{Pm})/2,\ A_{Sys} = \begin{bmatrix} \widehat{f_1} & \widehat{g_1} & \widehat{h_1} \end{bmatrix} \quad (4)$$

$$v_1 = p_{Al} - p_{Pm},\ v_2 = p_P - p_A,\ v_3 = v_2 \times v_1 \quad (5)$$

$$\widehat{h}_1 = v_1/|v_1|,\ \widehat{f}_1 = v_3/|v_3|,\ \widehat{g}_1 = \widehat{h}_1 \times \widehat{f}_1 \quad (6)$$

$$T_{Dia,G} = \begin{bmatrix} & A_{Dia} & & o_{Dia} \\ 0 & 0 & 0 & 1 \end{bmatrix} \quad (7)$$

where

$$o_{Dia} = (p_{Al'} - p_{Pm'})/2,\ A_{Dia} = \begin{bmatrix} \widehat{f}_2 & \widehat{g}_2 & \widehat{h}_2 \end{bmatrix} \quad (8)$$

$$v_4 = p_{Al'} - p_{Pm'},\ v_5 = p_{P'} - p_{A'},\ v_6 = v_5 \times v_4 \quad (9)$$

$$\widehat{h}_2 = v_4/|v_4|,\ \widehat{f}_2 = v_6/|v_6|,\ \widehat{g}_2 = \widehat{h}_2 \times \widehat{f}_2 \quad (10)$$

2.3. Dynamic annular motion

Dynamic annular motion was defined by applying time-varying nonlinear nodal displacement of the nodes along the annulus between the end of diastole and peak systole (Fig. 2B). The nonlinear annular displacement (**r**) was calculated by

$$\mathrm{r} = \mathrm{r}_{Dia} + w\mathrm{p} \quad (11)$$

where w is the time-varying scaled annular displacement and **p** is the direction vector from the nodal position at end diastole to that at peak systole ($\mathbf{r}_{Sys}\mathbf{r}_{Dia}$). The time-varying scaled annular displacement was calculated such that w=0 at end diastole and w=1 at peak systole, and the weight change was determined using previously reported ECG-gated annular motion data (Nguyen et al., 2008). The ECG-gated annular displacement data were resampled to determine nonlinear dynamic annular motion and coordinated with pressure gradient change across the MV over the cardiac cycle (dashed line, Fig. 3). Physiological transvalvular pressure gradient was applied to the ventricular side of both anterior and posterior leaflets allowing dynamic MV simulation (solid line, Fig. 3).

During MV function across the cardiac cycle, the PMs contract and stretch to retain the distance to the annulus as constant as possible (Dagum et al., 2000; Joudinaud et al., 2007). Therefore, PM contraction was modeled such that the location of PM tips dynamically deformed maintaining a constant distance from the top of the annulus during MV function.

2.4. Comparative studies of MV modeling

A total of five primary geometric parameters of the annular dimension were determined and compared between the 3D TEE data and the virtual MV models. Anterolateral-to-posteromedial diameter (DAlPm), anterior-to-posterior diameter (DAP), and annular perimeter (C3D) were determined by measuring distances between two points and along the annulus. Annular area (A2D) was calculated on the projection plane created from the annular curvature by the least square method. Annular height (H) was calculated by measuring the distance between the highest and lowest annular points with respect to the normal direction of the projection plane. A clinical MV quantitation software, QLAB-Mitral Valve Quantification (Philips Medical Systems, Bothell, WA), was utilized and the measured geometric information was compared with that from the virtual MV models.

2.5. Material modeling and contact conditions for dynamic MV simulation

The leaflet tissue was modeled as an anisotropic hyperelastic material using a Fung-type elastic constitutive model (Okamoto et al., 2003). In terms of Green-Lagrange strain (E), the Cauchy stress (σ) can be derived by

$$\sigma=\frac{1}{J}\mathrm{F}\frac{\partial W}{\partial E}\mathrm{F}^{T} \quad (12)$$

where J is the determinant of the deformation gradient (**F**). The Fung-type elastic constitutive model was defined using the following strain energy function W with four parameters (c, A_1, A_2 and A_3) (May-Newman and Yin, 1998).

$$W=\frac{c}{2}[e^{Q}-1], \qquad Q=A_1E_{11}^2+A_2E_{22}^2+2A_3E_{11}E_{22} \quad (13)$$

In a nearly incompressible hyperelastic material (J=det **F**=1), the stress–strain relationship is given by

$$\sigma_c=(2E_{11}+1)c\exp(Q)(A_1E_{11}+A_3E_{22}) \quad (14)$$

$$\sigma_r=(2E_{22}+1)c\exp(Q)(A_3E_{11}+A_2E_{22}) \quad (15)$$

This stress–strain relationship was defined along the circumferential (σ_c) and radial (σ_r) directions. Material parameters were determined by fitting biaxial mechanical test data of the anterior and posterior leaflet tissue from a previous study (May-Newman and Yin, 1998). The Levenberg–Marquardt nonlinear least squares algorithm was utilized for the curve fitting. The Fung-type elastic material model was implemented into ABAQUS/Explicit (SIMULIA, Providence, RI). Leaflet thickness was set to be 0.69 mm and 0.51 mm for the anterior and posterior leaflets, respectively (May-Newman and Yin, 1995).

The chordae tendineae were modeled as nonlinear hyperelastic materials using the 1st order Ogden model for the posterior marginal chordae and the 2nd order Ogden models for the anterior marginal and strut chordae (Prot et al., 2010). Cross-sectional areas were set 0.29 mm^2 for the anterior marginal chordae, 0.27 mm^2 for the posterior marginal chordae and 0.61 mm^2 for the strut chordae (Prot et al., 2010). Density and Poisson's ratio of the whole MV apparatus were set to be 1100 kg/m^3 and 0.48, respectively (Kim et al., 2007, 2008; Votta et al., 2007). Coaptation between two leaflets and self-contact in each leaflet were modeled using the general contact algorithm with the penalty method. The friction coefficient was assumed to be 0.05 (Stevanella et al., 2009). Coaptation lengths from the 3D TEE data and the corresponding dynamic MV simulation with and without consideration of annular motion were determined and compared.

We evaluated two sets of patient data based on the presence of MR. Change of annular morphology, stress distribution across the leaflets and annulus, and contact stress distribution were determined to assess the effect of annular motion on MV function and leaflet coaptation in patients with and without MR.

3. Results

3.1. Virtual MV modeling

Fig. 4A demonstrates volumetric MV morphology at peak systole and end diastole from 3D TEE image data. MV leaflets are clearly visible from the ventricular viewpoint. The corresponding virtual MV apparatus is shown in Fig. 4B demonstrating the anterior and posterior leaflets, annulus, marginal and strut chordae tendineae, and PM tips. No mesh distortion was observed.

Annular geometric parameters of the virtual MV model at end diastole and peak systole were compared with the original 3D TEE data (Table 1). The difference of annular geometric parameters between the 3D TEE data and the virtual MV models was less than 9%. This indicates that the annular shapes from the patient 3D TEE data at two different cardiac phases were successfully converted to virtual MV models using this custom-designed image processing algorithm.

3.2. Dynamic annular motion

Fig. 5 demonstrates dynamic motion of the annulus throughout the cardiac cycle. The annular shape change of the MV without regurgitation (Patient 1) demonstrated an increase of annular height in the mid-anterior region leading to a relatively symmetric saddle-shaped annular morphology at peak systole. DAlPm (commissure-to-commissure diameter) at end diastole (39.7 mm) was reduced by 12% at peak systole (35.0 mm) while the change of DAP was 7.2% (26.3 mm to 24.4 mm) (Table 1). The MV with regurgitation (Patient 2) demonstrated a relatively flatter annular shape (posterior view) across the cardiac cycle compared to Patient 1. The changes of annular shape in terms of both DAlPm (15%; 41.7 mm at end diastole to 35.4 mm at peak systole) and DAP (19%; 36.9 mm to 30.0 mm) were larger than Patient 1 (Table 1). The FE-predicted morphologies of the MV apparatus at end diastole (blue) and peak systole (red) are shown in Fig. 6. The MV without regurgitation (Patient 1) demonstrated an oval annular shape from the atrial view at both positions while an irregularly elongated annular shape was observed in the MV with regurgitation (Patient 2). An apparent saddle-shaped annulus was clearly observed at peak systole in Patient 1, whereas the change of annular height was smaller in Patient 2.

3.3. Evaluation of MV dynamics with and without annular motion

With the addition of dynamic annular motion, there was a substantial effect on the morphologic alteration and stress distribution across the MV leaflets. Stress distributions across the MV leaflets at peak systole calculated from MV simulations with and without dynamic annular motion are shown in Fig. 7. In order to provide a clear comparison of large stress distribution between the MV simulations, a threshold of stress value (0.4 MPa) was imposed such that larger stresses than the threshold value were displayed in red. MV simulations without annular motion demonstrated a wider range of regions with large stress values compared to MV simulations with annular motion.

When annular motion was not incorporated, the MV without regurgitation (Patient 1) demonstrated large stress values in the vicinity of the anterior saddle-horn where the largest bending occurred. The anterior leaflet displayed a reduced distribution of large stress values around the saddle-horn when annular motion was considered in the simulation while the posterior leaflet demonstrated a relatively considerable stress distribution. The maximum von Mises stress values with and without dynamic annular motion in Patient 1 were 0.7 MPa and 1.5 MPa respectively.

Reduction of large stress distribution across the MV leaflets by implementing dynamic annular motion was more noticeably demonstrated in simulations of the MV with regurgitation (Patient 2). Unlike the Patient 1 simulations, there was no difference in the maximum von Mises stress value (0.9 MPa) between the simulations with and without considering dynamic annular motion. There was a clear difference in large stress distribution between the simulations. Enhanced and extended distribution of large stress values from the saddle-horn region to the belly region were observed in the anterior leaflet when annular motion was not considered. However, the incorporation of dynamic annular motion resulted in markedly reduced stress distribution across both anterior and posterior leaflets. Interestingly, in the simulation without annular motion, the largest stress value appeared near the mid-posterior region and the anterolateral commissure. This posterior region with the largest stress value almost disappeared when annular motion was incorporated. In both anterior and posterior leaflets of Patient 2, large stress values spread out along the radial direction while Patient 1 showed a broader directional stress demonstration.

3.4. Contact stress distribution with and without annular motion

In order to evaluate the effect of dynamic annular motion on leaflet coaptation, contact stresses were computed at peak systole (Fig. 8). A threshold value was introduced to better demonstrate large contact stress values such that stress values larger than 10 kPa were displayed in red (full contact) and zero stress in blue (no contact). Consideration of annular motion resulted in increased leaflet coaptation in both patients. Patient 1 (without MR) showed sufficient leaflet coaptation regardless of considering annular motion while the total size of contact area was significantly increased when annular motion was incorporated. However, Patient 2 (with MR) demonstrated three non-contact regions between the leaflets in the simulation without annular motion. Two of these non-contact regions almost disappeared with the incorporation of realistic annular motion except the largest region in the mid-posterior marginal region.

3.5. Coaptation lengths and PM forces

We have conducted two comparative validation studies with respect to coaptation length and reaction force on the PM tips. MV simulations without the incorporation of annular motion demonstrated a difference of 8.0% and 35.5% in coaptation length compared with the 3D TEE data in patients with and without MR, respectively (Table 2). This difference in coaptation length decreased to 3.7% and 9.6%, respectively, when dynamic annular motion was incorporated into the MV simulations.

A previous in-vitro study experimentally measured the force of 4.5 N exerted on the PM tips at peak systole (120 mmHg) (Jensen et al., 2001). The average forces exerted on the PM tips at peak systole in the MV simulations with and without consideration of dynamic annular motion in the present study were 3.3±0.6 N and 4.3±1.1 N, respectively.

4. Discussion

Accurate evaluation of the effect of annular motion on MV dynamics has been one of the most popular but poorly understood issues in MV biomechanics. Studies have focused on optimization of the shape and dimension of the annulus utilizing ring annuloplasty to restore leaflet coaptation and normal mitral function (Rausch et al., 2011a, 2011b). Most FE simulation studies have used geometrically idealized MV models with representative geometric MV parameters (Prot et al., 2009; Salgo et al., 2002; Stevanella et al., 2009). Although these studies help us to understand the effect of annular motion on normal MV function, patient-specific information of MV geometry across the cardiac cycle is required to

better determine the extent and severity of abnormal MV function and better evaluate efficacy of mitral repair to restore normal MV function.

In this study, we developed a novel algorithm to incorporate patient-specific geometric changes of annular motion into a dynamic FE simulation of MV function. Dynamic annular motion was incorporated along with pressure gradient changes across the MV to calculate time-varying scaled annular displacement. In patients with and without MR, our simulations clearly demonstrated patient-specific deformation of annular shape across the cardiac cycle leading to substantial changes in stress distribution over the leaflets and annulus. Large stress values across the leaflets were reduced regardless of the presence of MR. This model suggests that simulation studies not considering patient-specific annular motion may lead to inaccurate stress prediction and misunderstanding of biomechanical changes in the MV structure. Additionally, the incorporation of dynamic annular motion clearly demonstrated an improved accuracy in determining the location of improper leaflet coaptation in patient with MR.

There are some factors that influenced our results. In this study, we utilized previously reported material property and leaflet thickness data of porcine MV tissue (May-Newman and Yin, 1998) to design the Fung-type elastic material model. Simulation results may differ if human tissue data are incorporated and should be interpreted in a qualitative manner. Since there are no actual data published for the in-plane shear components of porcine MV tissue, we modeled only normal components previously reported (May-Newman and Yin, 1998). Although we utilized leaflet geometry and dynamic annular motion from patient 3D TEE data to create a virtual MV model, the chordae tendineae and PM locations were modeled based on previously reported clinical data (Lam et al., 1970; Prot et al., 2010; Sonne et al., 2009). We are currently developing an improved MV modeling protocol to add more realistic chordae tendineae modeling and incorporate PM locations directly from patient 3D TEE data.

Additionally we are increasing the number of cases with and without MR to better confirm our results as to the importance of dynamic annular motion on MV function. However, in this study, we present solid data concerning the importance of the incorporation of patient-specific annular motion to accurate MV modeling.

This study demonstrates the effect of dynamic annular motion on computational studies of MV dynamics. This strategy has the potential to better quantitate the extent of pathologic alterations in the MV apparatus and better evaluate functional restoration following MV repair. potential to better quantitate the extent of pathologic alterations in the MV apparatus and better evaluate functional restoration following MV repair.

Acknowledgments

This work was in part supported by the National Institutes of Health (R01 HL109597, PI—Hyunggun Kim).

References

Carlhall C, Wigstrom L, Heiberg E, Karlsson M, Bolger AF, Nylander E. Contribution of mitral annular excursion and shape dynamics to total left ventricular volume change. American Journal of Physiology—Heart and Circulatory Physiology. 2004; 287:H1836–1841. [PubMed: 15205168]

Dagum P, Timek TA, Green GR, Lai D, Daughters GT, Liang DH, Hayase M, Ingels NB Jr, Miller DC. Coordinate-free analysis of mitral valve dynamics in normal and ischemic hearts. Circulation. 2000; 102:III62–III69. [PubMed: 11082364]

Ganapathy S. Decomposition of transformation matrices for robot vision. Proceedings of 2004 IEEE International Conference on Robotics and Automation. 1984; 1:130–139.

Gorman JH 3rd, Jackson BM, Enomoto Y, Gorman RC. The effect of regional ischemia on mitral valve annular saddle shape. Annals of Thoracic Surgery. 2004; 77:544–548. [PubMed: 14759435]

Hung J, Lang R, Flachskampf F, Shernan SK, McCulloch ML, Adams DB, Thomas J, Vannan M, Ryan T. 3D echocardiography: a review of the current status and future directions. Journal of the American Society of Echocardiography. 2007; 20:213–233. [PubMed: 17336747]

Jensen MO, Fontaine AA, Yoganathan AP. Improved in vitro quantification of the force exerted by the papillary muscle on the left ventricular wall: three-dimensional force vector measurement system. Annals of Biomedical Engineering. 2001; 29:406–413. [PubMed: 11400721]

Joudinaud TM, Kegel CL, Flecher EM, Weber PA, Lansac E, Hvass U, Duran CM. The papillary muscles as shock absorbers of the mitral valve complex. An experimental study. European Journal of Cardiothoracic Surgery. 2007; 32:96–101. [PubMed: 17512209]

Kim H, Chandran KB, Sacks MS, Lu J. An experimentally derived stress resultant shell model for heart valve dynamic simulations. Annals of Biomedical Engineering. 2007; 35:30–44. [PubMed: 17089074]

Kim H, Lu J, Sacks MS, Chandran KB. Dynamic simulation of bioprosthetic heart valves using a stress resultant shell model. Annals of Biomedical Engineering. 2008; 36:262–275. [PubMed: 18046648]

Lam JH, Ranganathan N, Wigle ED, Silver MD. Morphology of the human mitral valve. I. Chordae tendineae: a new classification. Circulation. 1970; 41:449–458. [PubMed: 5415982]

Lansac E, Lim KH, Shomura Y, Goetz WA, Lim HS, Rice NT, Saber H, Duran CM. Dynamic balance of the aortomitral junction. Journal of Thoracic and Cardiovascular Surgery. 2002; 123:911–918. [PubMed: 12019376]

Maffessanti F, Marsan NA, Tamborini G, Sugeng L, Caiani EG, Gripari P, Alamanni F, Jeevanandam V, Lang RM, Pepi M. Quantitative analysis of mitral valve apparatus in mitral valve prolapse before and after annulo-plasty: a three-dimensional intraoperative transesophageal study. Journal of the American Society of Echocardiography. 2011; 24:405–413. [PubMed: 21353470]

Maisano F, Redaelli A, Soncini M, Votta E, Arcobasso L, Alfieri O. An annular prosthesis for the treatment of functional mitral regurgitation: finite element model analysis of a dog bone-shaped ring prosthesis. Annals of Thoracic Surgery. 2005; 79:1268–1275. [PubMed: 15797061]

May-Newman K, Yin FC. Biaxial mechanical behavior of excised porcine mitral valve leaflets. American Journal of Physiology. 1995; 269:H1319–1327. [PubMed: 7485564]

May-Newman K, Yin FC. A constitutive law for mitral valve tissue. Journal of Biomechanical Engineering. 1998; 120:38–47. [PubMed: 9675679]

Nguyen TC, Itoh A, Carlhall CJ, Bothe W, Timek TA, Ennis DB, Oakes RA, Liang D, Daughters GT, Ingels NB Jr, Miller DC. The effect of pure mitral regurgitation on mitral annular geometry and three-dimensional saddle shape. Journal of Thoracic and Cardiovascular Surgery. 2008; 136:557–565. [PubMed: 18805251]

Okamoto RJ, Xu H, Kouchoukos NT, Moon MR, Sundt TM 3rd. The influence of mechanical properties on wall stress and distensibility of the dilated ascending aorta. Journal of Thoracic and Cardiovascular Surgery. 2003; 126:842–850. [PubMed: 14502164]

Paul, RP. Robot Manipulators: Mathematics, Programming, and Control. 4. MIT Press; 1981.

Prot V, Haaverstad R, Skallerud B. Finite element analysis of the mitral apparatus: annulus shape effect and chordal force distribution. Biomechanics and Modeling in Mechanobiology. 2009; 8:43–55. [PubMed: 18193309]

Prot V, Skallerud B, Sommer G, Holzapfel GA. On modelling and analysis of healthy and pathological human mitral valves: two case studies. Journal of the Mechanical Behavior of Biomedical Materials. 2010; 3:167–177. [PubMed: 20129416]

Rausch MK, Bothe W, Kvitting JP, Swanson JC, Ingels NB Jr, Miller DC, Kuhl E. Characterization of mitral valve annular dynamics in the beating heart. Annals of Biomedical Engineering. 2011a; 39:1690–1702. [PubMed: 21336803]

Rausch MK, Bothe W, Kvitting JP, Swanson JC, Miller DC, Kuhl E. Mitral valve annuloplasty: a quantitative clinical and mechanical comparison of different annuloplasty devices. Annals of Biomedical Engineering. 2011b; 40:750–761. [PubMed: 22037916]

Salgo IS, Gorman JH 3rd, Gorman RC, Jackson BM, Bowen FW, St Plappert T, John Sutton MG, Edmunds LH Jr. Effect of annular shape on leaflet curvature in reducing mitral leaflet stress. Circulation. 2002; 106:711–717. [PubMed: 12163432]

Sonne C, Sugeng L, Watanabe N, Weinert L, Saito K, Tsukiji M, Yoshida K, Takeuchi M, Mor-Avi V, Lang RM. Age and body surface area dependency of mitral valve and papillary apparatus parameters: assessment by real-time three-dimensional echocardiography. European Journal of Echo-cardiography. 2009; 10:287–294.

Stevanella M, Votta E, Redaelli A. Mitral valve finite element modeling: implications of tissues' nonlinear response and annular motion. Journal of Biomechanical Engineering. 2009; 131:121010. [PubMed: 20524733]

Sugeng L, Shernan SK, Weinert L, Shook D, Raman J, Jeevanandam V, DuPont F, Fox J, Mor-Avi V, Lang RM. Real-time three-dimensional transesophageal echocardiography in valve disease: comparison with surgical findings and evaluation of prosthetic valves. Journal of the American Society of Echocardiography. 2008; 21:1347–1354. [PubMed: 18848429]

Swaans MJ, Van den Branden BJ, Van der Heyden JA, Post MC, Rensing BJ, Eefting FD, Plokker HW, Jaarsma W. Three-dimensional transoeso-phageal echocardiography in a patient undergoing percutaneous mitral valve repair using the edge-to-edge clip technique. European Journal of Echocardiography. 2009; 10:982–983. [PubMed: 19654135]

Votta E, Maisano F, Bolling SF, Alfieri O, Montevecchi FM, Redaelli A. The Geoform disease-specific annuloplasty system: a finite element study. Annals of Thoracic Surgery. 2007; 84:92–101. [PubMed: 17588392]

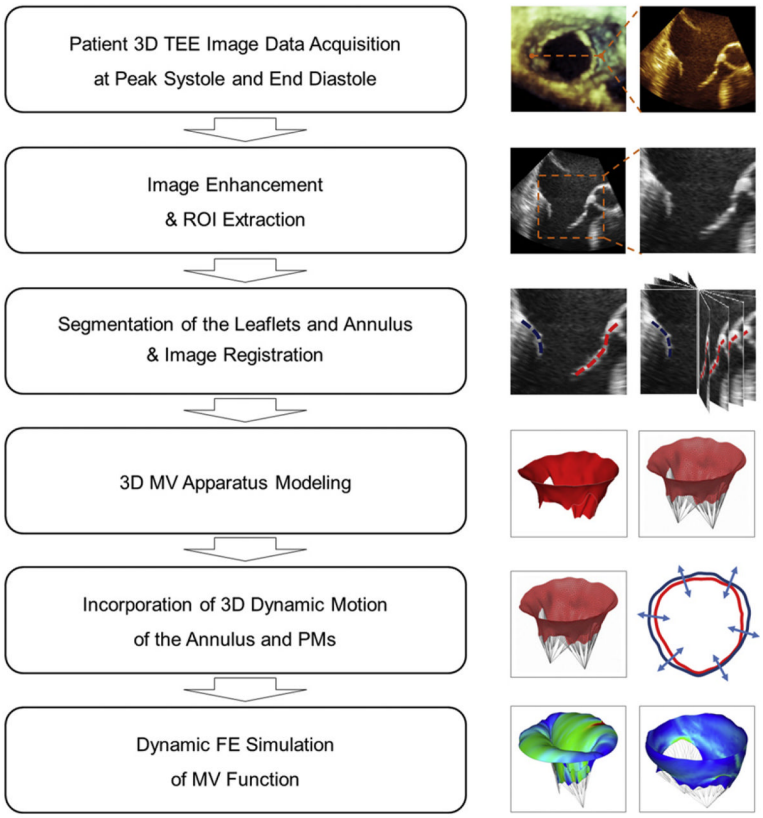

Fig. 1.

Study protocol for MV modeling and dynamic annular motion using patient 3D TEE data followed by dynamic FE simulation.

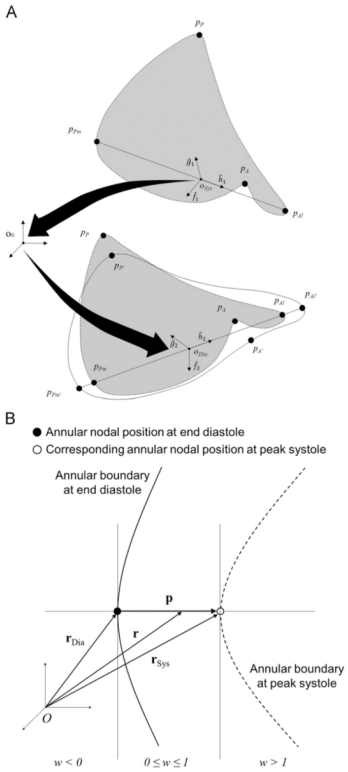

Fig. 2.

(A) Transformation system between the two annular configurations. At peak systole (O_{Sys}): p_{Al}—anterolateral commissure point, p_{Pm}—posteromedial commissure point, p_A—midpoint of the anterior annulus, p_P—midpoint of the posterior annulus. At end diastole (O_{Dia}): $p_{Al'}$—anterolateral commissure point, $p_{Pm'}$—posteromedial commissure point, $p_{A'}$ – midpoint of the anterior annulus, $p_{P'}$—midpoint of the posterior annulus. (B) Nonlinear nodal displacement of the annulus from end diastole to peak systole calculated using the time-varying scaled annular displacement and the direction vector.

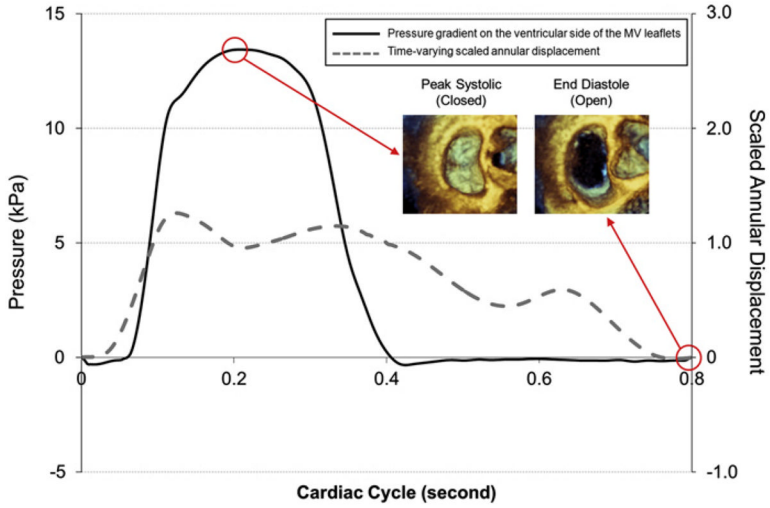

Fig. 3.

Transvalvular pressure gradient across the MV and ECG-gated time-varying scaled annular displacement imposed.

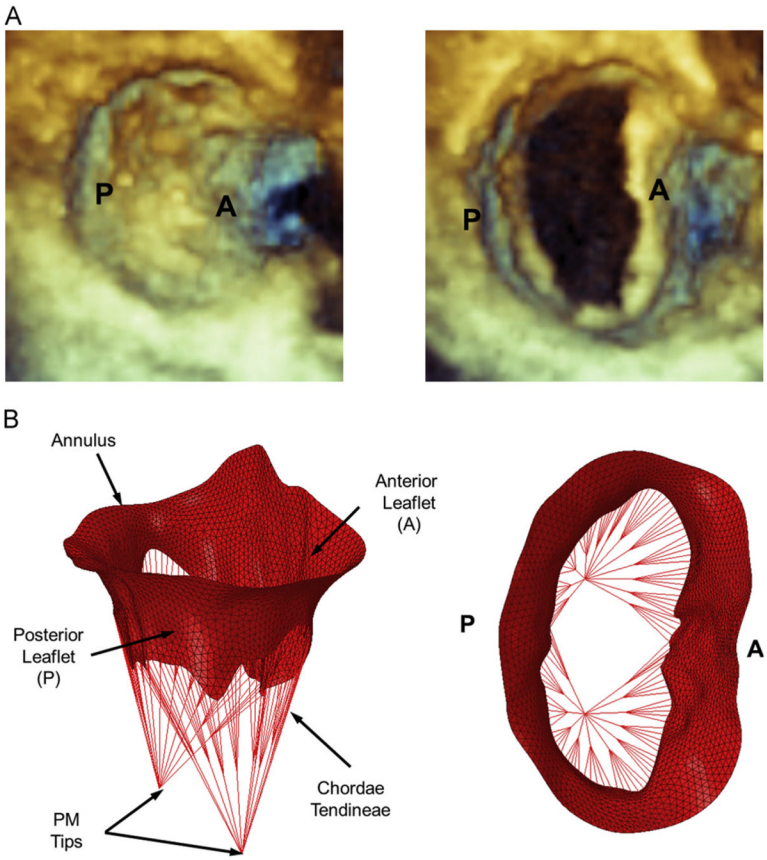

Fig. 4.

(A) Volumetric MV images from 3D TEE data demonstrating MV morphology at peak systole and end diastole (ventricular view). (B) Corresponding images of the virtual MV model demonstrating the anterior and posterior leaflets, annulus, marginal and strut chordae tendineae, and the PM tips.

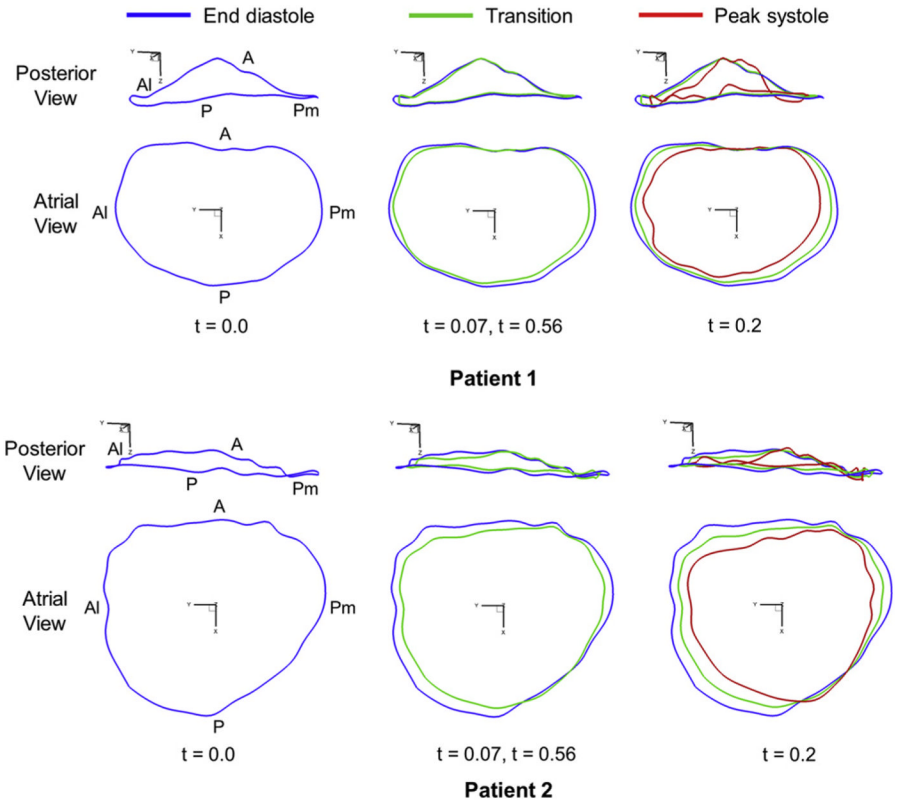

Fig. 5.

Dynamic motion of the annulus across the cardiac cycle. Annular shapes are displayed from the posterior and atrial viewpoints in each patient data to demonstrate and compare dynamic annular motion between the patients. (For interpretation of the references to color in this figure legend, the reader is referred to the web version of this article.)

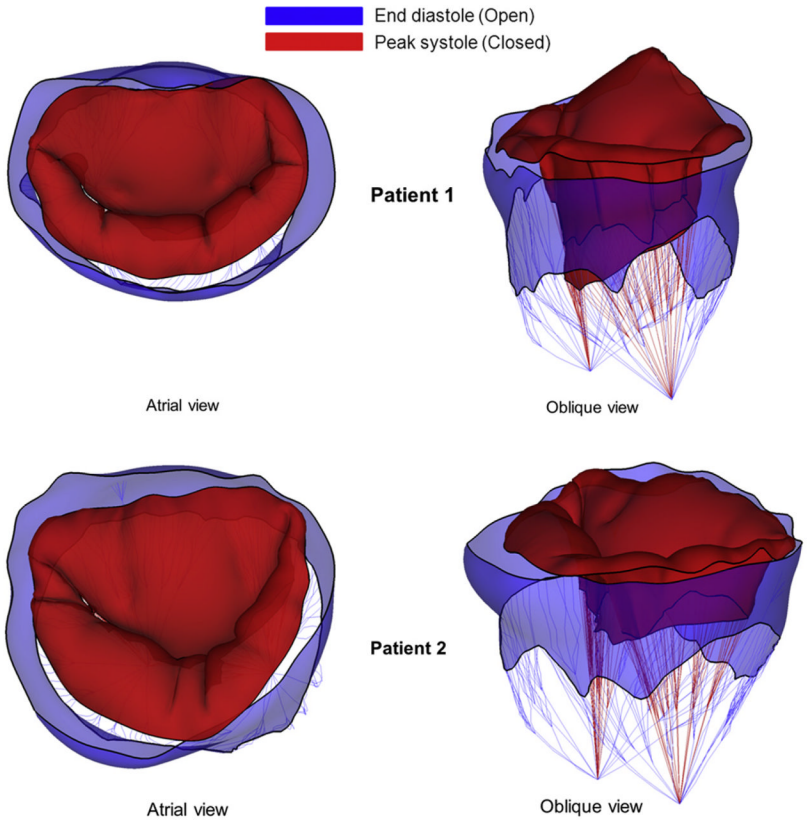

Fig. 6.

Morphology of the MV apparatus at end diastole and peak systole demonstrating dynamic annular motion as well as leaflet deformation. (For interpretation of the references to color in this figure legend, the reader is referred to the web version of this article.)

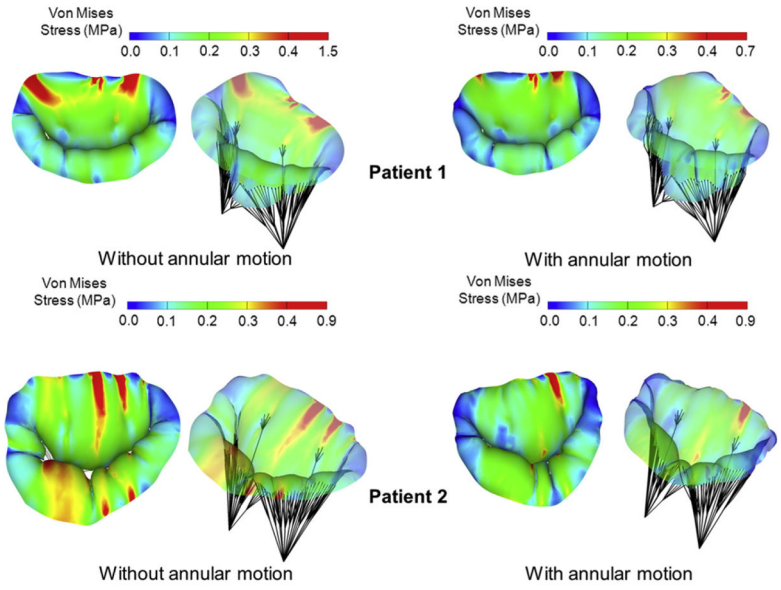

Fig. 7.

Von Mises stress distribution across the MV leaflets and annulus at peak systole with and without dynamic annular motion.

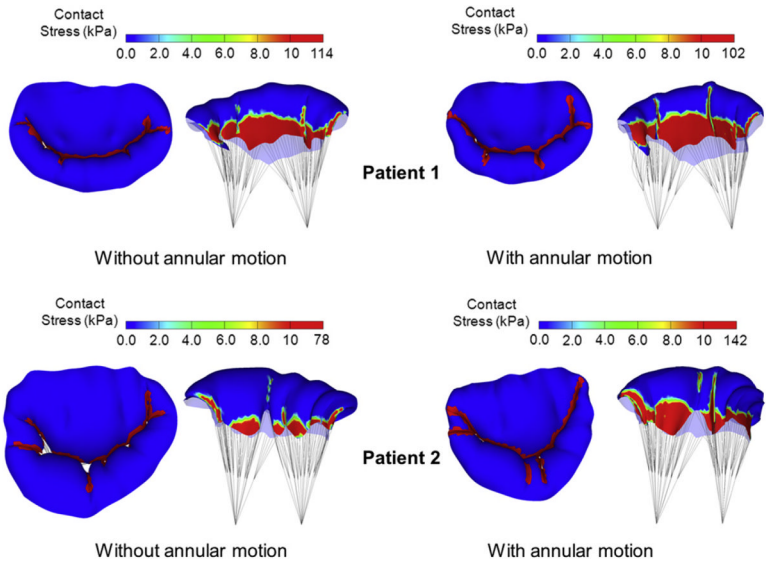

Fig. 8.

Contact stress distribution across the MV leaflets at peak systole demonstrating the effect of dynamic annular motion on contact evaluation in patient with MR.

Table 1

Comparison of annular geometries between the 3D TEE data and the virtual MV model.

Case	Cardiac cycle	Geometric parameters	3D TEE data from clinical software (repeated 3 measurements)	3D MV model	Difference (%)
MV without Regurgitation (Patient 1)	End of Diastole	DAlPm (mm)	42.3±0.8	39.7	6.1
		DAP (mm)	25.8±0.4	26.3	1.9
		H (mm)	6.7±0.3	7.2	7.5
		C3D (mm)	120±1.6	114	5.0
		A2D (mm^2)	905±21	921	1.8
	Peak Systole	DAlPm (mm)	36.2±0.5	35.0	3.3
		DAP (mm)	25.8±0.5	24.4	5.4
		H (mm)	8.6±0.8	9.1	5.8
		C3D (mm)	107±0.6	108	1.0
		A2D (mm2)	747±21	714	4.4
MV with Regurgitation (Patient 2)	End of Diastole	DAlPm (mm)	42.7±1.8	41.7	2.3
		DAP (mm)	35.8±0.2	36.9	3.1
		H (mm)	4.6±0.1	4.3	6.5
		C3D (mm)	125±3.2	131	4.8
		A2D (mm^2)	1175±51	1249	6.3
	Peak Systole	DAlPm (mm)	37.2±0.6	35.4	4.8
		DAP (mm)	31.4±0.4	30.0	4.5
		H (mm)	5.5±0.2	5.8	5.5
		C3D (mm)	118±1.4	115	2.5
		A2D (mm2)	9727±15	888	8.7

DAlPm—anterolateral-to-posteromedial annular diameter, DAP—anterior-to-posterior annular diameter, H—annular height, C3D—annular perimeter, A2D—annular area on the projection plane

Table 2

Coaptation lengths from the 3D TEE data and dynamic MV simulation.

Case	3D TEE data from clinical software (repeated 3 measurements)	Incorporation of annular motion	Dynamic MV simulation	Difference (%)
MV without regurgita- tion (Patient 1)	43.771.5	No	47.2	8
		Yes	42.1	3.7
MV with regurgita- tion (Patient 2)	44.872.4	No	60.7	35.5
		Yes	49.3	9.6